Direct PSF Estimation Using a Random Noise Target

Johannes Brauers, Claude Seiler and Til Aach

Institute of Imaging and Computer Vision, RWTH Aachen University
Templergraben 55, 52056 Aachen, Germany

ABSTRACT

Conventional point spread function (PSF) measurement methods often use parametric models for the estimation of the PSF. This limits the shape of the PSF to a specific form provided by the model. However, there are unconventional imaging systems like multispectral cameras with optical bandpass filters, which produce an, e.g., unsymmetric PSF. To estimate such PSFs we have developed a new measurement method utilizing a random noise test target with markers: After acquisition of this target, a synthetic prototype of the test target is geometrically transformed to match the acquired image with respect to its geometric alignment. This allows us to estimate the PSF by direct comparison between prototype and image. The noise target allows us to evaluate all frequencies due to the approximately "white" spectrum of the test target – we are not limited to a specifically shaped PSF. The registration of the prototype pattern gives us the opportunity to take the specific spectrum into account and not just a "white" spectrum, which might be a weak assumption in small image regions. Based on the PSF measurement, we perform a deconvolution. We present comprehensive results for the PSF estimation using our multispectral camera and provide deconvolution results.

Keywords: point spread function, deconvolution, noise target, registration, multispectral imaging

1. INTRODUCTION

Several methods for measuring the modulation transfer function (MTF), which is the frequency domain representation of the PSF, are available:[1] A complex and expensive method utilizing wavefront analysis with an interferometer using a laser source as a monochromatic light source computes the PSF by a Fourier transformation of the measured pupil wavefront. Other methods are based on the acquisition of a back-illuminated pinhole or knife-edge: Under the assumption of an infinitesimally small pinhole, the acquired image directly represents the PSF of the system. In practice, the pinhole is modeled as a disc and the differing input pattern has to be taken into account. Making the hole as small as possible reduces the available light and causes serious problems with the signal to noise ratio. An edge spread function may be derived by imaging a knife-edge. A derivation of the resulting image gives the one-dimensional line spread function in one particular direction. By rotating the knife-edge, a derivation of the two-dimensional PSF is possible. While the method using an interferometer is very expensive, the others require the acquisition of multiple images or are limited by the available light.

In the ISO 12233 specification,[2] the MTF measurement with respect to the quality assessment of a camera and a lens is performed with a test chart showing sine waves with several frequencies and orientations. A measurement of the contrast of these patterns depending on the orientation and frequency allows a computation of the MTF. The measurement is extended to several image locations by Loebich et al.[3] However, both methods do not allow the computation of the PSF since they sample the MTF only at a few discrete orientations. While their intention is the measurement of an MTF with a fine frequency resolution, we are interested in the estimation of the full two-dimensional PSF.

Other approaches[4,5] acquire a test chart with known spatial content and compute the PSF or MTF by comparing the acquired image with the test chart. The estimation is done either in the frequency domain (MTF) or in the spatial domain (PSF). Methods in the frequency domain perform a division of the frequency spectrum of the acquired image by the one of the template. Approaches in the spatial domain mostly utilize a PSF model function and fit its model parameters by minimizing an energy term: Mansouri et al.[6] use a disc shaped PSF to

Further author information: (Send correspondence to Johannes Brauers.)
Johannes Brauers: E–mail: Johannes.Brauers@lfb.rwth-aachen.de, Telephone: +49 (241) 80 27866

Digital Photography VI, edited by Francisco Imai, Nitin Sampat, Feng Xiao, Proc. of SPIE-IS&T Electronic Imaging,
SPIE Vol. 7537, 75370B · © 2010 SPIE-IS&T · CCC code: 0277-786X/10/$18 · doi: 10.1117/12.837591

estimate the blurring produced by the optical filters of a multispectral camera – the only parameter is the size of the disc. Wei et al.[7] utilize a Gaussian-shaped PSF with several parameters to characterize stray light and to reduce it finally. The model assumptions may be valid for some cases and allow a stable estimation, since only a few parameters have to be estimated.

However, parameterized models for the PSF are not valid for, e.g., our multispectral camera[8,9] shown in Fig. 1: Inside our camera, a filter wheel with optical bandpass filters is placed between the lens and the sensor. As we will show in section 2, the optical filters cause a position-dependent PSF, which cannot be parameterized with a simple model function. To a certain degree, this also holds for the system without optical filters and may apply for other camera systems, too. Our context for PSF estimation is the separate characterization of each passband of our multispectral camera: Since the optical bandpass filters differ in their optical properties like their refraction indices and thicknesses, the images acquired with some optical bandpass filters are slightly blurred.[10] Our aim is to measure the PSF and to recover the original sharpness.

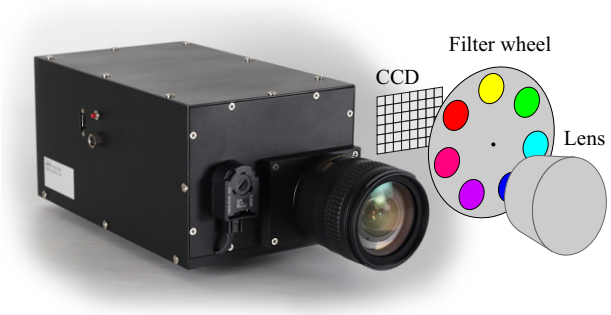

Figure 1. Our multispectral camera with its internal configuration sketched.

To cope with the arbitrarily shaped PSFs, we use a non-parameterized PSF estimation, i.e., we estimate the optical transfer function (OTF) in the spectral domain and transform it to the spatial domain to obtain the PSF. The approach by Levy et al.[11] utilizes a test chart shown on a computer monitor, which is acquired by the tested camera and lens. However, the computed PSF is not space-resolved but applies for the whole image. The same holds for the work of Trimeche et al.,[5] where a checkerboard pattern is used as a template for PSF estimation. Joshi et al.[4] account for the spatial dependency of the PSF and utilize a test chart with a circular checkerboard pattern. However, as we will show in section 2, this pattern does not exhibit an (approximately) flat frequency spectrum and may have inferior performance with respect to PSF estimation.

In the following section, we will describe the background and underlying principle of PSF estimation. In section 3, we present our algorithm for PSF estimation including the regularization of the PSF. We show results in the forth section before we conclude in the last section.

2. PHYSICAL BACKGROUND

To be independent of measurements of point spread functions (PSF) with a real lens and to have still an idea of the form of the PSF, we simulated an optical system which is similar to our real system: Fig. 2 shows the optical layout of a lens[12] which has the same focal length range and a similar optical layout compared to our lens (Nikon Nikkor AF-S DX 18-70mm). We included an optical bandpass filter, which is used in our multispectral camera to subdivide the visible electromagnetic spectrum. The filter has a refraction index $n = 2.05$ and a thickness $d = 5\,\text{mm}$. We focused the imaging system by optimizing the image distance and therefore minimized the size of the airy discs on the image surface.

Fig. 3 shows the simulated point spread functions for various positions in the image plane, where each accumulation of points represents one PSF. It can be seen that mostly, the shape of the PSFs does not exhibit a radial symmetry and does not resemble a Gaussian shape. In addition, the PSFs depend on their spatial

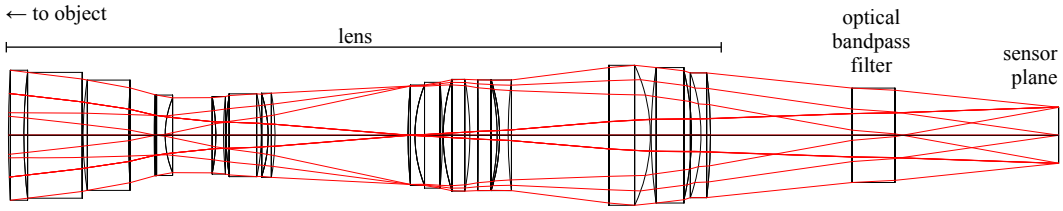

Figure 2. Lens design[12] similar to the lens in our multispectral camera with additional optical bandpass filter. Three object rays are simulated.

position. Therefore, it is crucial to account for a shift-variant PSF which is not restricted to a specific form. It can be modeled by

$$i(x,y) = \sum_{x_0,y_0} h\left(x,y;x_0,y_0\right) \cdot o\left(x_0,y_0\right) + n(x,y)\ , \tag{1}$$

where the original image is denoted by $o(x,y)$ and the blurred image by $i(x,y)$. The spatially varying point spread function is given by $h(x_0,y_0;x,y)$, yielding a specific PSF for each spatial image position x,y. Additional noise is modeled by $n(x,y)$.

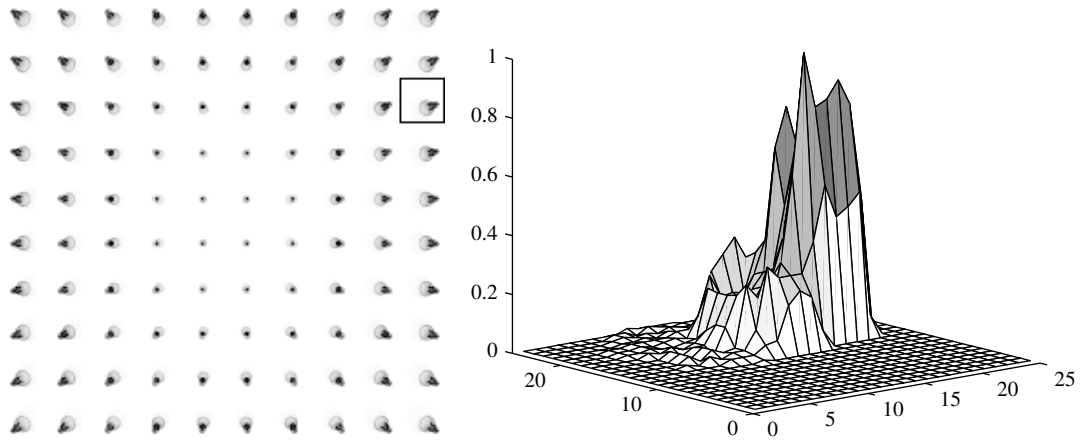

(a) (b)

Figure 3. Blockwise PSF computation (a) performed by the optical simulation program ZEMAX using the lens from Fig. 2; each spot represents one PSF. The spatial dependency of the single PSFs can be clearly seen. The form of a specific PSF (b) does not exhibit a radial symmetry and does not resemble a simple Gaussian shape or disc shape.

Since it is not feasible to take a separate PSF for each pixel into account and because neighboring point spread functions are considered to be similar, we split the image into blocks (96×80 pixel) and use one PSF for each image block. Most of the following operations are therefore performed blockwise, i.e., the processing is described for one image block and applies for the others analogously. Eq. (1) therefore reduces to

$$i(x,y) = \left(p * o\right)(x,y) + n(x,y) \tag{2}$$

and

$$I(u,v) = P(u,v)O(u,v) + N(u,v) \tag{3}$$

in the frequency domain. Here, the capital identifiers correspond to the lower case ones and $P(u,v)$ is the optical

transfer function (OTF) of the system. The OTF is then estimated in the frequency domain via

$$\hat{P}(u,v) = \frac{I(u,v)}{\hat{O}(u,v)} \tag{4}$$

by the division of the acquired image by the estimated original image $\hat{O}(x,y)$ in the frequency domain. The estimation of $\hat{O}(x,y)$ is discussed in section 3.

Several templates may be used to perform the PSF measurement. The checkerboard pattern in Fig. 4c is usually utilized in geometric camera calibration tasks. Trimeche et al.[5] use it as a template for the PSF measurement. However, its frequency spectrum shown in Fig. 4d is inhomogeneous and exhibits frequency components near zero. These components appear in the denominator of Eq. (4) and prevent or at least complicate a reliable estimation of the OTF. Fig. 4a is an improved version of the checkerboard pattern presented by Joshi et al.,[4] which exhibits all orientations of an edge but still has crossings which can be used for geometric calibration. However, the frequency domain still shows an inhomogeneous distribution.

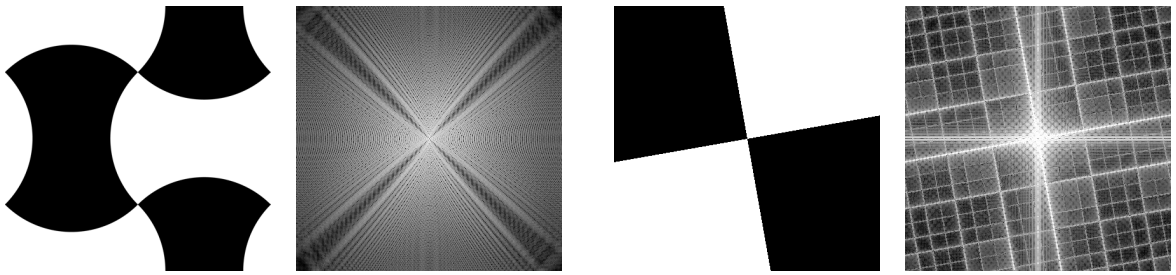

(a) (b) (c) (d)

Figure 4. Templates for PSF estimation from Joshi et al.[4] and Trimeche et al.[5] are shown in (a) and (c), respectively. The subfigures (b) and (d) show the corresponding frequency domain representation (scaled logarithmically), which is inhomogeneous in both cases.

We use the template shown in Fig. 5, which exhibits white uniform noise in the background and some registration markers and a gray wedge in the foreground. We acquire a part in the center of the test chart including the markers. Since white noise in the spatial domain transforms to white noise in the frequency domain as well, the frequency spectrum of our target is homogeneous and does not exhibit components near zero like the other charts shown in Fig. 4. The markers in the image are very small and do not tamper the homogeneity of the spectrum.

The resolution of the test chart is a crucial aspect: If the resolution is too coarse, some frequency components are missing and the optical transfer function cannot be estimated in these frequency bands. If the resolution is too fine, the energy of the test chart is truncated by the lowpass of the optics. This causes a reduced contrast in the image and the signal to noise ratio (SNR) of the image is reduced, too. We have chosen a one-to-one relation between pixels on the template and the acquired image as a compromise. Since the lens and the bandpass filter represent to a certain degree a spatial lowpass filter, we expect the sampling theorem not to be violated.

3. ESTIMATION ALGORITHM FOR THE PSF

Our algorithm for PSF estimation is illustrated in Fig. 6 and estimates the point spread function (PSF) from the acquired image and a digital template (see Fig. 5). First of all, the digital template is geometrically registered with the acquired image. Towards this end, the markers in the acquired image are detected and their positions are used to compute a preliminary geometric transformation between the acquired image and the digital template as indicated by dashed lines in Fig. 5. We have chosen a projective transformation[13] which allows a scaling, rotation and projective distortion between both images. To refine the transformation, we compute a subpixel-precise displacement vector field[9] between both images, starting from the transformation computed above. Combining both registration methods, we transform the digital template to match the acquired image geometrically. The

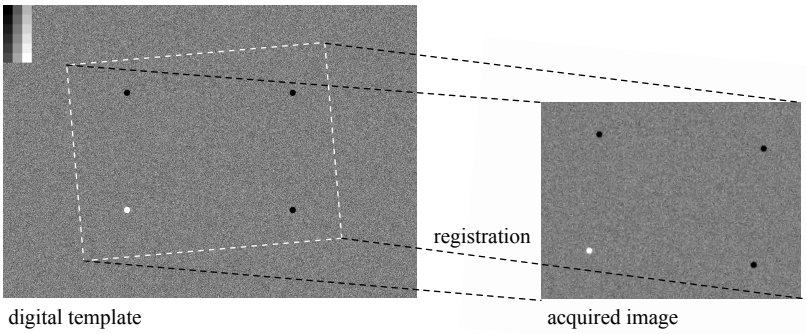

Figure 5. Our noise target with localization markers and gray patches (left) is geometrically registered with the acquired image.

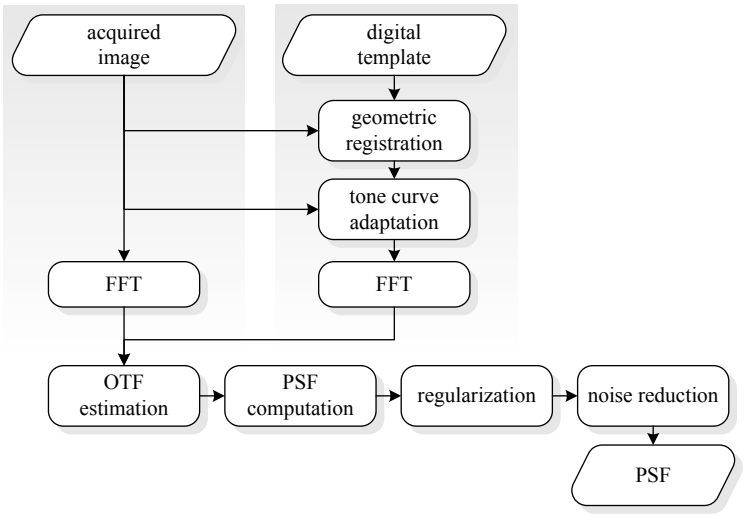

Figure 6. The proposed PSF estimation algorithm.

remaining differences concern the intensity, noise and sharpness of the image: Since the acquired image has been acquired utilizing a real lens and a camera, it is not as sharp as the transformed digital template.

In the next step *tone curve adaptation*, we compute a tone curve describing the relation between the intensity levels from the digital template and the acquired image. By doing so, we account for non-linear tone curves of the camera and the printer, although we did our best to get linear curves. To measure the combined tone curve, we utilize the gray wedge in the top left corner of our test chart, which has to be acquired separately. (The printer is assumed to exhibit a constant tone curve over the whole image.) We extract an averaged value of each gray patch and set the value into relation with the original value, which finally results in the combined tone curve. We then adapt the brightness levels of the digital template to the acquired image by applying the tone curve.

After that, the images are split into small image blocks (96×80 pixel) and the fast Fourier transformation (FFT) is used to transform them to the frequency domain. The OTF can then be computed using Eq. (4) and the PSF is derived by an inverse FFT. Since our test chart consists of white noise, one might expect that it is necessary to assume a constant frequency spectrum instead of using a complex registration algorithm to estimate the frequency spectrum. However, since the estimation of the PSF is performed on small blocks with 7680 pixel values, this assumption is not given. In other words, the exact noise pattern in the examined region has to be known.

Because the image is divided into image blocks, the number of pixels contributing to the estimation of the

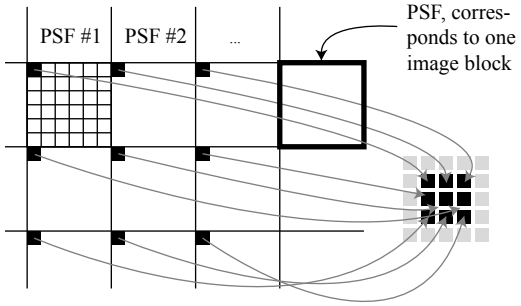

Figure 7. Basic principle for regularization of PSFs: the same pixels of each PSF are combined to a new block, to which the filter operations are applied to.

PSF is reduced compared to an estimation taking all pixels of the image into account and thus the stability of the estimation is decreased. We therefore developed an algorithm which performs a regularization between neighboring PSFs. In the following, we assume that the optical system only changes slowly and neighboring PSFs are similar. The basic principle is shown in Fig. 7: The PSFs for different image blocks are arranged consecutively in a new image. The pixel at same position within each PSF are then rearranged to a new block. For example, the right block in the figure is composed of the top left pixel of each PSF. Each one of these blocks is then processed with filters and rearranged to its previous arrangement. The filtering includes a 3×3 median filter, which reduces stochastic errors between neighboring blocks: If the PSF estimation fails in one block and, e.g., produces abnormal pixel values, the PSF data is taken from neighboring PSFs. The following lowpass filter with the filter kernel

$$H = \begin{pmatrix} 1 & 2 & 1 \\ 2 & 4 & 2 \\ 1 & 2 & 1 \end{pmatrix} \tag{5}$$

ensures a certain smoothness between neighboring PSFs and reduces noise, too.

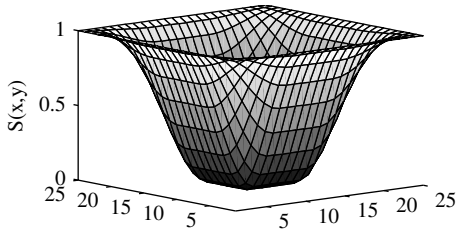

Figure 8. Window for the reduction of PSF noise.

The last operation is a thresholding operation, where the pixel values of the PSF below a certain location-dependent threshold are set to zero. This reduces the noise near the border of a PSF, where only small values are expected. The thresholding window (see Fig. 8) is defined by

$$S(x, y) = 1 - T(x)T(y) \tag{6}$$

and the Tukey window[14]

$$T(n) = \begin{cases} 1 & \text{for } 0 \leq |n| \leq \alpha\frac{N}{2} \\ 0.5\left[1 + \cos\left(\pi\frac{n-\alpha\frac{N}{2}}{2(1-\alpha)\frac{N}{2}}\right)\right] & \text{for } \alpha\frac{N}{2} \leq |n| \leq \frac{N}{2} \end{cases} \tag{7}$$

where N is the size of the window. We chose the Tukey window since the width of the tip of the window can be

adjusted by the parameter α. The thresholding operation is then performed by

$$p(x,y) = \begin{cases} 0 & \text{for } \tilde{p}(x,y) < \tilde{p}_{\max} S(x,y) \\ \tilde{p}(x,y) & \text{otherwise} \end{cases} \tag{8}$$

where $\tilde{p}_{\max}$ is the maximum value of the unfiltered PSF $\tilde{p}(x,y)$ for each block and $p(x,y)$ the result of the operation. Finally, we normalize the PSF to make the sum of its coefficients equal to one.

4. RESULTS

We performed the PSF measurement using our seven-channel multispectral camera[8,9] with a Nikon Nikkor AF-S DX 18-70mm lens. The internal grayscale camera is a Sony XCD-SX900 with a chip size of 6.4 mm×4.8 mm, a resolution of 1280×960 pixel and a pixel pitch of 4.65 μm × 4.65 μm. The lens has an F-mount known from single lens reflex (SLR) cameras, whereas the camera has a C-mount, which is often used for industrial cameras. The optical filters in our camera span a wavelength range from 400 nm to 700 nm with a bandwidth of 40 nm each and a wavelength distance of 50 nm.

Fig. 9 shows the result of the tone curve measurement (see Fig. 6): A curve of the form $y = ax^b + c$ (solid line) has been fitted the measurement points (dots) with the parameters $a = 0.93$, $b = 0.97$, $c = 28$. The parameter $b \approx 1$ indicates that there is almost a linear relation between the gray values of the template and the ones acquired from the printed test target. The high black level of $c = 28$ is noticeable; however, the camera itself exhibits a black level near the gray value 10.

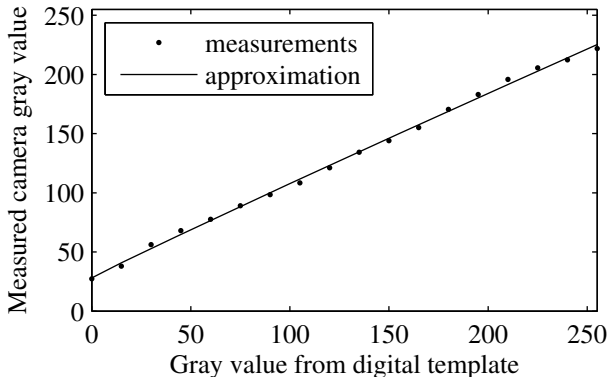

Figure 9. Tonecurve between original digital calibration target and its printed and acquired version.

The results of the regularization in Fig. 10 show that the noise in the original PSF (Fig. 10a) can be greatly reduced by averaging the PSF with neighboring PSFs (Fig. 10b). The thresholding operation further reduces the noise – especially in border regions – and gives the final result shown in Fig. 10c.

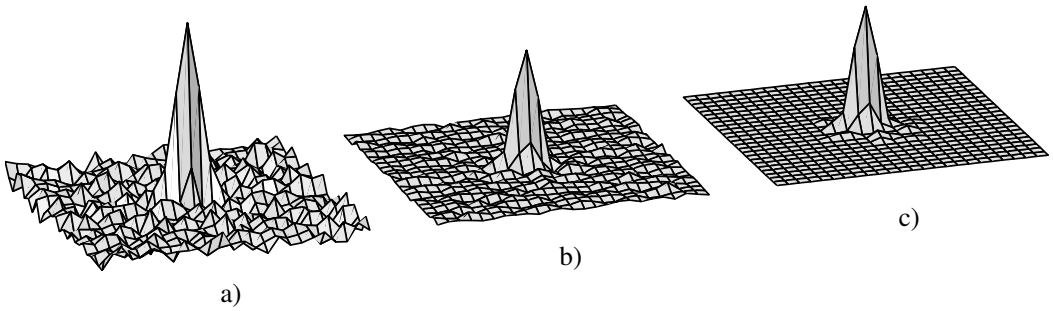

Figure 10. Regularization of the measured PSF (a) with mean/median filtering (b) and thresholding (c).

Fig. 11 shows the blockwise PSF measurement for our multispectral camera when the 700 nm bandpass filter has been selected: Each box in the figure represents one PSF for the corresponding image block. The spatial dependency observed in the second section of this paper is indicated by a position-dependent shape of the PSF. A more detailed view of the marked PSF is presented in Fig. 12a: The PSF shown here does neither exhibit a radial symmetry, nor resemble a Gaussian shaped PSF. Therefore, a simple PSF model (e.g., Gaussian) is not suited to model the PSF. Fig. 12b shows the same region when the 550 nm bandpass filter is selected in our camera. Since we focused the camera's lens using this passband, the PSF is much smaller – which corresponds to a sharper image.

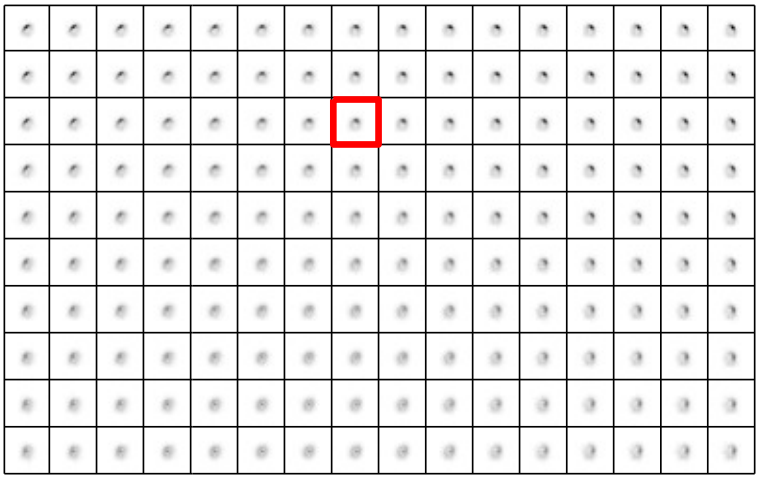

Figure 11. Blockwise PSF estimation for the 700 nm passband; each box shows the PSF of its corresponding image block. A 3D plot for the marked region is given in Fig. 12.

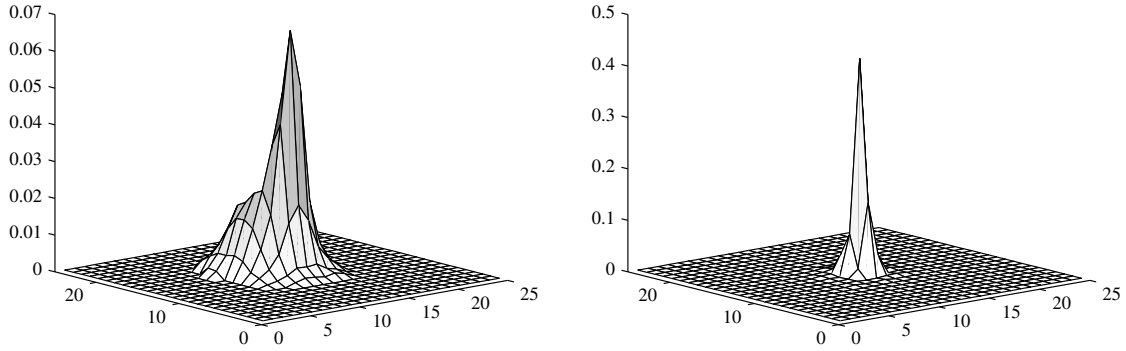

(a) 700 nm passband (b) 550 nm passband

Figure 12. Detailed PSFs for the marked block in Fig. 11 for two passbands.

To validate the PSF estimation, we also performed a deconvolution using the above estimated PSF. We used the random test target with markers to produce the image in Fig. 13: The left area shows a crop of the acquired image, which is quite blurry. The lower right crop presents the synthetic prototype, which has been registered to match the acquired image geometrically. It is used to estimate the PSF – together with the acquired image. The upper crop shows the deconvolution result, where the sharpness of the original image has approximately been restored. For deconvolution, we used the algorithm from Levin et al.[15]

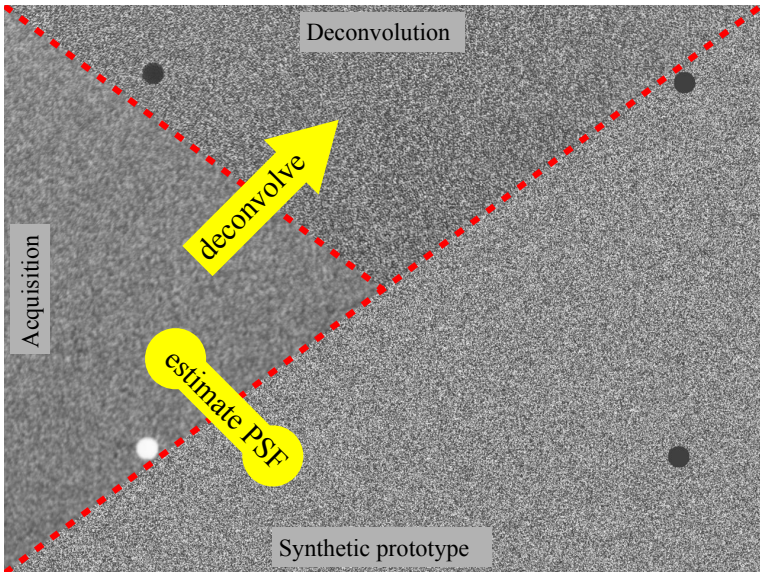

Figure 13. Our random noise calibration target in three different versions: The PSFs are estimated utilizing the synthetic prototype and the acquired image and are used to deconvolve the acquired image.

5. CONCLUSIONS

By performing a simulation of an optical system, we have shown an example for a spatially varying PSF which has a shape of considerable complexity and cannot be characterized with a simple model function. We discussed the frequency spectrum properties of some test charts for PSF estimation and presented our own target with white noise and some additional markers. Based on this chart, we described our PSF estimation algorithm including a registration and linearization of the template with respect to the acquired image. The proposed regularization technique reduces noise and ensures a smooth transition between neighboring PSFs. Our PSF measurements confirm the assumption of an asymmetric and spatially varying PSF. A deconvolution with the measured PSF shows that the sharpness of the image can be clearly enhanced.

ACKNOWLEDGMENTS

The authors acknowledge gratefully funding by the German Research Foundation (DFG, grant AA5/2-1).

REFERENCES

[1] Wilcox, M., "How to measure MTF and other properties of lenses," tech. rep., Optikos Corporation, 286 Cardinal Medeiros Ave Cambridge, MA 024141 USA (July 1999).

[2] "Electronic still-picture cameras resolution measurements." ISO12233:2000(E) (2000).

[3] Loebich, C., Wueller, D., Klingen, B., and Jaeger, A., "Digital camera resolution measurement using sinusoidal siemens stars," in [*IS&T/SPIE Electronic Imaging*], 65020N–1–65020N–11 (Jan 2007).

[4] Joshi, N., Szeliski, R., and Kriegman, D. J., "PSF estimation using sharp edge prediction," in [*IEEE Conference on Computer Vision and Pattern Recognition, CVPR*], 1–8 (23-28 June 2008).

[5] Trimeche, M., Paliy, D., Vehvilainen, M., and Katkovnic, V., "Multichannel image deblurring of raw color components," in [*IS&T/SPIE Electronic Imaging*], Bouman, C. A. and Miller, E. L., eds., **5674**, 169–178, SPIE (March 2005).

[6] Mansouri, A., Marzani, F. S., Hardeberg, J. Y., and Gouton, P., "Optical calibration of a multispectral imaging system based on interference filters," *SPIE Optical Engineering* **44**, 027004.1–027004.12 (Feb 2005).

[7] Wei, J., Bitlis, B., Bernstein, A., de Silva, A., Jansson, P. A., and Allebach, J. P., "Stray light and shading reduction in digital photography - a new model and algorithm," in [*IS&T/SPIE Electronic Imaging*], (Jan 2008).

[8] Brauers, J., Schulte, N., Bell, A. A., and Aach, T., "Multispectral high dynamic range imaging," in [*IS&T/SPIE Electronic Imaging*], **6807** (Jan 2008).

[9] Brauers, J., Schulte, N., and Aach, T., "Multispectral filter-wheel cameras: Geometric distortion model and compensation algorithms," *IEEE Transactions on Image Processing* **17**, 2368–2380 (Dec 2008).

[10] Brauers, J. and Aach, T., "Longitudinal aberrations caused by optical filters and their compensation in multispectral imaging," in [*IEEE International Conference on Image Processing (ICIP2008)*], 525–528 (CD–ROM), IEEE, San Diego, CA, USA (Oct 2008).

[11] Levy, E., Peles, D., Opher-Lipson, M., and Lipson, S. G., "Modulation transfer function of a lens measured with a random target method," *Applied Optics* **38**, 679–683 (Feb 1999).

[12] Hayakawa, S., "Zoom lens system." Patent (Mar 2005). US. Pat. 2005/0068636 Al.

[13] Hartley, R. I. and Zisserman, A., [*Multiple View Geometry in Computer Vision*], Cambridge University Press, ISBN: 0521540518, second ed. (2004).

[14] Harris, F., "On the use of windows for harmonic analysis with the discrete fourier transform," *Proceedings of the IEEE* **66**(1), 51–83 (1978).

[15] Levin, A., Fergus, R., Durand, F., and Freeman, W. T., "Deconvolution using natural image priors," (2007). http://groups.csail.mit.edu/graphics/CodedAperture/SparseDeconv-LevinEtAl07.pdf.